



Gas-particle partitioning of atmospheric reactive mercury and its contribution to particle bound mercury in a coastal city of the Yangtze River Delta, China

Lingling Xu^{a,b,**}, Yanru Zhang^{a,b,c}, Lei Tong^{a,b}, Yuping Chen^{a,b,c}, Guoqing Zhao^{a,b}, Youwei Hong^{a,b}, Hang Xiao^{a,b}, Jinsheng Chen^{a,b,*}

^a Center for Excellence in Regional Atmospheric Environment, Institute of Urban Environment, Chinese Academy of Sciences, Xiamen, 361021, China

^b Key Lab of Urban Environment and Health, Institute of Urban Environment, Chinese Academy of Sciences, Xiamen, 361021, China

^c University of Chinese Academy Sciences, Beijing, 100049, China

HIGHLIGHTS

- Speciated Hg, meteorology, and aerosol compositions were synchronously observed.
- RM partitioning strongly depended on temperature in the colder season.
- Effects of aerosol compositions on RM partitioning were discussed.
- Relative contribution of RM partitioning to PBM in different seasons was determined.

ARTICLE INFO

Keywords:

Atmospheric reactive mercury
Gas-particle partitioning
Temperature
Aerosol compositions
PCA-MLR

ABSTRACT

Speciated atmospheric mercury including reactive gaseous mercury (RGM), particle bound mercury (PBM), and gaseous elemental mercury (GEM) were measured for a two-year period in Ningbo city, the Yangtze River Delta, China. Averaged concentrations of PBM and RGM were $316 \pm 377 \text{ pg m}^{-3}$ and $100 \pm 123 \text{ pg m}^{-3}$, respectively, with the highest RGM/PBM ratio in summer (0.73 ± 1.31) and the lowest in winter (0.35 ± 0.56). The relationship between RGM/PBM ratio and $\text{PM}_{2.5}$ was nonlinear. When $\text{PM}_{2.5}$ fell in the range of $15\text{--}100 \text{ }\mu\text{g m}^{-3}$, the PBM increased, the RGM decreased, and the RGM/PBM ratio showed an obvious decreasing trend as $\text{PM}_{2.5}$ increased. An empirical linear relationship between $\log(1/K_p)$ and $1/T$ was obtained for different seasons. The correlation coefficient and slope of the equation were highest in winter, suggesting that T explained more for K_p variation and RM transferred quickly to the particle phase in the cold season. The relationships between K_p and aerosol compositions show that K_p increased with increasing fractions of Organics (Org), nitrate (NO_3), and chloride (Chl) and decreasing fractions of sulfate (SO_4) and ammonium (NH_4) in aerosols. Principle component analysis - multiple linear regression (PCA-MLR) was used to evaluate the relative contributions of gas-particle partitioning of RM and sectional primary emissions to PBM in different seasons. The results show that the contributions of RM partitioning to PBM were 28.0% in spring, 28.3% in summer, 31.2% in autumn, and 39.2% in winter, which was well explained by the seasonal variations of temperature and aerosol compositions.

1. Introduction

Atmospheric mercury (Hg) exist as two forms of gaseous elemental

mercury (GEM) and reactive mercury (RM, or oxidized Hg). RM in gas and particle phases are often known as reactive gaseous mercury (RGM) and particle bound mercury (PBM) respectively, which were widely

* Corresponding author. Center for Excellence in Regional Atmospheric Environment, Institute of Urban Environment, Chinese Academy of Sciences, Xiamen, 361021, China.

** Corresponding author. Center for Excellence in Regional Atmospheric Environment, Institute of Urban Environment, Chinese Academy of Sciences, Xiamen 361021, China.

E-mail addresses: linglingxu@iue.ac.cn (L. Xu), jschen@iue.ac.cn (J. Chen).

<https://doi.org/10.1016/j.atmosenv.2020.117744>

Received 31 March 2020; Received in revised form 23 June 2020; Accepted 24 June 2020

Available online 13 July 2020

1352-2310/© 2020 Elsevier Ltd. All rights reserved.

determined by Hg collected on a denuder coated with KCl and on a downstream quartz filter (Landis et al., 2002). RM contributed generally less than 5% of total atmospheric Hg (Schroeder and Munthe, 1998), but in the Arctic, the contribution could be up to 100% (Gustin et al., 2015; Steffen et al., 2015). RM still plays an important role in Hg cycle. Due to its high water solubility and high chemical reactivity, RM is the main Hg species entering aquatic systems via wet and dry depositions. Consequently, it can be transformed into a more toxic form, methylmercury (MeHg), that is potentially harmful to human health (Schroeder and Munthe, 1998; AMAP and UNEP, 2013). Moreover, the gaseous and particulate RM are removed from the atmosphere via different physical processes and deposited with different rates (Seinfeld and Pandis, 2006). Hence, understanding the characteristics of RM in the atmosphere is essential to estimate Hg deposition and to assess atmospheric Hg exposure.

Levels of PBM and RGM in the atmosphere are mainly controlled by primary emissions, GEM oxidation processes, gas-particle partitioning, and depositions (Zhang et al., 2013; Qin et al., 2019). Since GEM accounts for majority of Hg in the atmosphere, RGM formed by GEM oxidation and RGM distribution to particle phase can significantly affect RGM and PBM concentrations. Gas-particle partitioning of RM is an inter-conversion process and was generally described as a partition coefficient (K_p). Rutter and Schauer (2007a) first found that the gas-particle partitioning of RM in both ambient and laboratory conditions was strongly temperature dependent and the relationship between K_p and temperature was similar to polycyclic aromatic hydrocarbons partitioning (Pankow, 1992). Many later studies have confirmed the influence of temperature on partition coefficients (Amos et al., 2012; Cheng et al., 2014; Lee et al., 2016; Zhang et al., 2019). RM partitioning was also found to be affected by aerosol chemical compositions in a laboratory study (Rutter and Schauer, 2007b). That study indicated that nitrate and chloride particles had a high partition coefficient, while ammonium sulfate had a low coefficient. However, the field research about this issue is very limited (Duan et al., 2016; Zhang et al., 2019) because aerosol chemical compositions are difficult to obtain.

Knowledge of RM partitioning in gas and particle phases is significant for Hg chemical transport models. Previous atmospheric Hg models assumed that RM partitioning between gas and particle phases should be a fixed ratio (Holmes et al., 2010; Bash et al., 2014), which is not consistent with the real atmosphere. Up to now, gas-particle partitioning of RM was studied mainly in North America (Amos et al., 2012; Cheng et al., 2014) and sporadically in Korea and China (Lee et al., 2016; Zhang et al., 2017a, 2019). Empirical coefficients of RM partitioning in various regions are necessary to evaluate the models' accuracy. What's more, a recent study conducted in Beijing found that the coefficient of RM partitioning differed among the seasons. This suggests that there is a great need to improve our understanding of RM partitioning in different seasons (Zhang et al., 2019).

In China, the total Hg emission from anthropogenic sources was estimated to be $\sim 500 \text{ t yr}^{-1}$ (AMAP and UNEP 2013; Zhang et al., 2015). The Yangtze River Delta (YRD) region is one of the heaviest Hg polluted areas in China due to its dense industries (Zhang et al., 2015). The anthropogenic emission of RGM ($108 \mu\text{g m}^{-2}$) was about 20 times higher than PBM emissions ($5.1 \mu\text{g m}^{-2}$) in the YRD region. However, lower atmospheric concentrations of RGM compared to PBM are widely reported in the YRD region, like Shanghai (Duan et al., 2017; Qin et al., 2019) and Ningbo (Hong et al., 2016). The results suggest an important contribution of gas-particle partitioning to atmospheric PBM. In this study, we presented the distribution of RM between gas and particle phases based on two years observation of speciated Hg in a coastal city of the YRD region; investigated how temperature and aerosol chemical compositions affect gas-particle partitioning of RM; and more importantly, we evaluated the relative contribution of RM partitioning to PBM compared to primary emissions in different seasons.

2. Experiment

2.1. Site description

Atmospheric speciated mercury were measured on the rooftop of a 15 m tall building of the Urban Environment Observation and Research Station in Beilun District, Ningbo, China (121.91° E , 29.87° N , Fig. S1). Ningbo is located in the YRD region and on the east coast of China, closely linking the Pacific Ocean. A large coal-fired power plant (5000 MW) is located 21 km northwest of the sampling site and a Chlor-alkali plant is located 22 km northeast of the site. An automobile assembly plant is located within 1 km of the site. Ningbo features a subtropical monsoon climate. The weather is relatively moderate with a perennial mean temperature of 16.4° C (the highest in July and the lowest in January) and a mean precipitation of 1480 mm. The prevailing wind in Ningbo is from the southeast in summer and from the northwest in winter.

2.2. Observation and data description

2.2.1. Speciated Hg analysis

Long term observations of GEM, PBM, and RGM were conducted using an automated Tekran 2537b/1130/1135 system (Tekran Inc., Toronto, Canada). A detailed description of this instrument can be found in previous studies (Xu et al., 2015; Hong et al., 2016). This study focused more on PBM and RGM concentrations directly associated with gas-particle partitioning of RM, while GEM was not the major species adsorbing onto particles (Schroeder and Munthe, 1998). A number of studies have indicated large discrepancies in PBM and RGM measurements by different collection and detection methods (Talbot et al., 2011; Huang et al., 2013). However, the uncertainties in PBM and RGM measurements can not be well quantified, because chemical forms of oxidized Hg are not clear and there is a lack of acceptable calibration methods (Jaffe et al., 2014; Gustin et al., 2015). Up to now, the Tekran system is the most common method, especially being adopted by monitoring networks worldwide. Keeping the bias derived from Tekran system in mind, this study tried to interpret the distribution of RM in gas and particle phases qualitatively based on a large amount of data. The time resolution of PBM and RGM concentrations was 2 h, with 1 h for sampling and the following 1 h for analysis. Strict QA/QC measures were taken for the Tekran system. The Tekran analyzer underwent routine internal calibration with Hg permeation source every day and external calibration with a Tekran 2505 every year. The KCl-coated annular denuder was replaced bi-weekly and the quartz filter was replaced monthly. PBM and RGM concentrations during the year of 2015 and 2017 were analyzed in this study and the data under method detection limit (MDL) (1.25 pg m^{-3} , Hong et al., 2016) were excluded from the analysis.

2.2.2. Air pollutants and meteorology

Concentrations of SO_2 , CO, NO_2 and O₃ were measured by Model 43i, 48i, 42i, and 49i, respectively (Thermo-Fisher Scientific Inc., USA). The gas analytic systems were calibrated every 2–3 weeks and a zero check was made for the CO analyzer every week. The systems pre-filter was replaced every 10–30 days. Concentrations of PM_{2.5} and PM₁₀ were determined by a TEOM R&P 1400 sampler (Thermo-Fisher Scientific Inc., USA) with a mass resolution of $0.01 \mu\text{g m}^{-3}$ and precisions of $\pm 1.5 \mu\text{g m}^{-3}$ (1 h average) and $\pm 0.5 \mu\text{g m}^{-3}$ (24 h average). The flow rate was monitored and calibrated every month. The TEOM filter was exchanged when the filter loading percentage was greater than 90%. Temperature (T) and relative humidity (RH) were monitored by an automatic weather station (WS500-UMB, Lufft, Germany) with precisions of $\pm 0.2^\circ \text{ C}$ and $\pm 2\%$, respectively.

2.2.3. Aerosol compositions analysis

Chemical compositions of non-refractory PM₁ (NR-PM₁, with an

aerodynamic diameter < 1 μm) derived from an Aerodyne aerosol chemical speciation monitor (ACSM) were used in this study as no data of $\text{PM}_{2.5}$ chemical compositions were available. Aerosol chemical compositions were measured during January ~ May 2015 and July ~ December 2017 covering four seasons. A detailed description of ACSM can be found in the previous study (Sun et al., 2012). Major chemical components included organics (Org), sulfate (SO_4), nitrate (NO_3), ammonium (NH_4), and chloride (Chl). Before analysis, the data of aerosol compositions were processed as 2 h averages to match the sampling interval of RM.

2.3. Regression models development

2.3.1. RM gas-particle partitioning coefficient (K_p)

Gas-particle partitioning of RM is expressed as a partition coefficient (K_p) which is determined by the RGM, PBM, and $\text{PM}_{2.5}$ concentrations. We used this equation to calculate K_p ($\text{m}^3 \mu\text{g}^{-1}$) (Rutter and Schauer, 2007a):

$$K_p = (\text{PBM}/\text{PM}_{2.5})/\text{RGM} \quad (1)$$

where $\text{PM}_{2.5}$ is the mass of $\text{PM}_{2.5}$ ($\mu\text{g m}^{-3}$), PBM and RGM are the concentrations of RM (pg m^{-3}) in $\text{PM}_{2.5}$ and in the gas phase, respectively. In this study, K_p derived from the 2 h average concentrations of RGM, PBM, and $\text{PM}_{2.5}$.

2.3.2. K_p – Temperature model

Previous studies have applied regression models to examine the relationship between K_p and T , and a linear regression model between $\log(1/K_p)$ and $1/T$ was widely used (Rutter and Schauer, 2007a; Cheng et al., 2014). We used this linear equation:

$$\text{Log}(1/K_p) = a + b(1/T) \quad (2)$$

where a and b are coefficients, T is the atmospheric temperature (K). A total of 6078 paired $\log(1/K_p)$ and $1/T$ data were obtained. In order to describe how K_p changes with T , the T bins averaging method (Cheng et al., 2014) was applied. The temperature ranged from -2.0 °C to 34.5 °C was set to each 1 °C bin. T bins with more than 10 K_p values were used in the linear regression analysis.

2.4. PCA-MLR

In this study, principle component analysis - multiple linear regression (PCA-MLR) was conducted to explore the factors influencing PBM. Air pollutants concentrations (SO_2 , NO_2 , CO, and PM), PBM and K_p were used in PCA. Kaiser-Meyer-Olkin (KMO) and Bartlett's tests were

applied to the data before factor analysis. The KMO test was larger than 0.5 and Bartlett's test was lower than 0.001, indicating that the data were suitable for factor analysis. Furthermore, the PCA factor scores were taken as independent variables and the z-score of PBM as dependent variables. MLR was further performed to assess the relative contribution of RM partitioning to PBM in different seasons.

3. Results and discussion

3.1. Characteristics of reactive mercury (RM)

Average concentrations of GEM, PBM, RGM, and air pollutants and the ratio of RGM/PBM in different seasons are summarized in Table 1. The average concentrations (\pm standard deviation) of GEM, PBM, and RGM were $2.6 \pm 1.0 \text{ ng m}^{-3}$, $316 \pm 377 \text{ pg m}^{-3}$, and $100 \pm 123 \text{ pg m}^{-3}$ during the whole study period, respectively. The concentration of PBM was the highest in winter, the lowest in summer, and moderate in spring and autumn. Similar seasonal variation was observed in these air pollutants, SO_2 , NO_2 , PM_{10} , and $\text{PM}_{2.5}$. As previous studies reported, increased PBM in winter could be attributed to suppressed air diffusion, intense combustion for residential heating, and enhanced gas-particle partitioning of RM due to low temperature (Rutter and Schauer, 2007a; Qin et al., 2019). The concentration of RGM was highest in spring. Similar seasonal pattern was also observed in Xiamen and Beijing, China and New York State, US (Choi et al., 2013; Xu et al., 2015; Zhang et al., 2019). The higher O_3 in spring could partly contribute to the enhanced photo-oxidation of GEM to RGM, which is backed up by a closer correlation between RGM and O_3 in spring than in other seasons (Table S1). Generally, the photo-oxidation of GEM was enhanced in warm seasons (spring and summer) due to the strong solar radiation and rich oxidants. However, the removal of RGM associated with more rain in summer probably resulted in the lower RGM in summer (Choi et al., 2013).

The ratio of RGM/PBM was 0.53 ± 0.86 in average, indicating that PBM accounted for two thirds of total RM in the atmosphere. RGM/PBM ratio varied largely among locations. The value of this study was lower than those reported from Canada (0.89 and 0.92), USA (0.62–2.57) and Korea (0.73–1.14) and those from remote and island areas of China (0.84 in Mt. Changbai and 1.35 in Dianshan Lake), but generally higher than those conducted in urban areas of China (such as 0.10 in Guiyang and 0.22 in Beijing) (Table S2). The results imply that RM was more dominated by particle phase than gas phase in regions with elevated particle pollution. The RGM/PBM ratio in Ningbo was the highest in summer (0.73 ± 1.31), followed by autumn (0.58 ± 0.71) and spring (0.45 ± 0.65), and the lowest in winter (0.35 ± 0.56). The distance of anthropogenic emission sources would change RGM/PBM ratio because

Table 1

Statistics for bi-hourly GEM, PBM and RGM concentrations, the ratio of RGM/PBM, air pollutants concentrations, temperature (T) and relative humidity (RH) during the study period.

	Spring		Summer		Autumn		Winter		Whole period	
	Mean	SD ^a	Mean	SD	Mean	SD	Mean	SD	Mean	SD
GEM (ng m^{-3})	2.7	0.9	2.4	0.8	2.6	1.0	2.8	1.1	2.6	1.0
PBM (pg m^{-3})	348	322	164	192	290	420	510	467	316	377
RGM (pg m^{-3})	122	169	72.9	88	98	100	102.8	98.1	100.0	123
RGM/PBM	0.45	0.65	0.73	1.31	0.58	0.71	0.35	0.56	0.53	0.86
SO_2 ($\mu\text{g m}^{-3}$)	11.0	4.5	8.4	4.6	9.2	5.9	12.7	9.8	10.3	6.7
NO_2 ($\mu\text{g m}^{-3}$)	22.9	13.1	12.7	7.7	25.3	16.6	37.4	21.5	24.5	17.8
CO (mg m^{-3})	0.49	0.20	0.50	0.15	0.82	0.34	0.97	0.61	0.69	0.42
O_3 ($\mu\text{g m}^{-3}$)	95.6	37.7	85.9	42.7	80.3	41.9	57.9	31.1	80.0	41.0
PM_{10} ($\mu\text{g m}^{-3}$)	45.3	27.0	33.1	17.9	43.0	27.4	68.1	50.6	47.4	35.3
$\text{PM}_{2.5}$ ($\mu\text{g m}^{-3}$)	26.6	14.4	20.4	11.8	25.4	17.0	40.9	31.7	28.3	21.6
T (°C)	15.3	4.8	25.9	3.0	20.1	4.9	8.4	3.3	17.5	7.6
RH (%)	85.1	14.5	92.7	7.3	84.5	12.7	75.8	17.1	84.6	14.6

^a SD is the standard deviation.

the residence time of RGM is generally shorter than PBM (Lee et al., 2016; Qin et al., 2019). According to a recent study, the GEM at the study site was strongly contributed by local and regional emission sources, such as the nearby industrial activities, the northwestern coal-fired power plant, and the transport from surrounding provinces with large amount of Hg emissions, while the contribution of long range transport was small (Yi et al., 2020). Thus, it could be speculated that the local/regional emission sources were the important contributors to RGM and PBM in the study area. Significant positive correlations of RGM and PBM with SO₂ ($r = 0.32$ and 0.43 , $p < 0.01$, Table 2) support the speculation. Anthropogenic sources have different speciated Hg profiles that affect the concentrations of RGM and PBM in the atmosphere. GEM is considered to be mainly from primary emissions. In this study, the ratio of RGM/PBM was negatively correlated with GEM ($r = -0.37$, $p < 0.01$, Table 2). Since anthropogenic emissions of RGM is much higher than PBM according to Hg emission inventory in China (Zhang et al., 2015), the negative correlation between RGM/PBM ratio and GEM was probably due to the conversion of RGM to PBM.

RM can be re-distributed between gas and particle phases once it emits to the atmosphere. Previous studies indicated that the concentration of PM_{2.5} might affect the formation of PBM via adsorption of RGM onto particles (Qin et al., 2019; Zhang et al., 2019). In this study, the ratio of RGM/PBM was negatively correlated with PM_{2.5} overall ($r = -0.41$, $p < 0.01$, Table 2). Moreover, the RGM/PBM ratio was averaged at each 2 h PM_{2.5} concentration and the graph revealing the relationship between RGM/PBM and PM_{2.5} was plotted. As showed in Fig. 1, when PM_{2.5} concentration was lower than 15 $\mu\text{g m}^{-3}$, the RGM, PBM, and RGM/PBM ratio all increased with increasing PM_{2.5}, suggesting a dominant influence of primary emissions. When PM_{2.5} fell in the range of 15–100 $\mu\text{g m}^{-3}$, the PBM increased, the RGM decreased, and the RGM/PBM ratio showed an obvious decreasing trend as PM_{2.5} increased. The phenomenon was probably due to the enhanced conversion of RGM to PBM. When PM_{2.5} exceeded 100 $\mu\text{g m}^{-3}$, the RGM/PBM ratio varied slightly as PM_{2.5} increased. Therefore, it is proposed that the gas-particle partitioning of RM plays a vital role in variations of RGM and PBM when the concentration of PM_{2.5} was approximately 15–100 $\mu\text{g m}^{-3}$. A similar concentration threshold (105 $\mu\text{g m}^{-3}$) was observed in Shanghai, East China (Qin et al., 2019). In following sections, we would like to discuss the factors influencing the gas-particle partitioning of RM and to evaluate the contribution of RM partitioning on PBM in different seasons.

3.2. Gas-particle partitioning of RM

K_p was used for describing RM gas-particle partitioning in the atmosphere. Using equation (1), average K_p in Ningbo was $0.24 \pm 0.43 \text{ m}^3 \mu\text{g}^{-1}$ over the whole study period. It was comparable to the value in Beijing ($0.20 \pm 0.25 \text{ m}^3 \mu\text{g}^{-1}$, Zhang et al., 2019), and some of the values in North America ($0.20\text{--}0.36 \text{ m}^3 \mu\text{g}^{-1}$, Cheng et al., 2014). In this study, the K_p values were significantly different among the seasons (K-W ANOVA test, $P < 0.001$). As showed in Fig. S2, the K_p values were higher in winter than in other seasons on the whole, with median values of 0.16, 0.15, 0.12, and 0.17 $\text{m}^3 \mu\text{g}^{-1}$ in spring, summer, autumn, and winter, respectively. The emission sources of atmospheric Hg might impact the seasonality of K_p , because they strongly affected PBM and

Table 2
Spearman correlations of PBM, RGM, and RGM/PBM ratio with other pollutants.

Species	PBM	RGM	RGM/PBM
GEM	0.392	0.010 ^a	-0.367
SO ₂	0.432	0.323	-0.102
NO ₂	0.358	0.143	-0.194
CO	0.263	0.046	-0.214
O ₃	0.065	0.153	0.106
PM ₁₀	0.546	0.130	-0.379
PM _{2.5}	0.542	0.098	-0.410

^a Correlation is not significant, while others are significant at $p < 0.01$ level.

RGM concentrations which directly involved in K_p calculation. In Beijing, K_p was firstly calculated in different seasons and showed higher values in autumn and winter than in spring and summer (Zhang et al., 2019). The difference of K_p among the seasons in Ningbo was not as remarkable as that in Beijing, which might be due to the minor seasonal difference of temperature in Ningbo. Moreover, RM partitioning was widely reported to be a function of temperature and related to aerosol chemical compositions (Rutter and Schauer, 2007a).

3.2.1. Impact of temperature on RM partitioning

The whole paired 2 h $K_p - T$ data were applied to the empirical regression model, yielding an equation of $\log(1/K_p) = (-1034 \pm 169)(1/T) + (4.4 \pm 0.6)$ ($R^2 = 0.59$, $P < 0.001$, Fig. 2a). Some studies have found that K_p increased with RH in colder seasons and in high humidity environments (Lyman and Keeler, 2005; Liu et al., 2010). So, paired $K_p - RH$ data were also treated similarly to paired $K_p - T$ data. Specifically, RH was set to each 1% bin and the bins with less than 10 K_p values were omitted. The relationship of K_p with RH was tested as $\log(1/K_p) = a + b RH$ but no significant correlation was found ($R^2 = 0.0075$, $P = 0.23$). Therefore, T , rather than RH, was the limited meteorological factor of RM partitioning. Previous studies also have reported that gas-particle partitioning of RM was a function of temperature (Rutter and Schauer, 2007a; Amos et al., 2012; Cheng et al., 2014; Han et al., 2014; Lee et al., 2016; Zhang et al., 2019).

The generated regression equation of this study and those reported from previous studies are summarized in Table 3. An inverse correlation between K_p and T (Fig. 2a) indicates that RM would partition from gas to particle phase with decreasing temperature. The correlation coefficient of K_p and T was 0.59, which means temperature explained ~59% of the variance in K_p . Rutter and Schauer (2007a) found the K_p values derived from filter-based method more depended on temperature than those from Tekran method; and attributed it to internal heating (50 °C) of Tekran sampling system. Compared the studies all using Tekran method, we found that temperature explained a comparable variance in K_p in America ($R^2 = 0.49\text{--}0.55$) and less K_p variance in Beijing, China ($R^2 = 0.24$). The slope of the $\log(1/K_p)$ model represents a change in the rate of RM partitioning with temperature. The slope was $-1034 \pm 169 \mu\text{g K m}^{-3}$ in this study, which was similar to that reported from Beijing (Zhang et al., 2019) and 2–4 times lower than those conducted in America (Rutter and Schauer, 2007a; Amos et al., 2012; Cheng et al., 2014).

In this study, we found that the points featured by high temperature (low $1/T$) obviously deviated from the fitting line (Fig. 2a). Hence, linear regression analysis was performed throughout the four seasons corresponding to distinct temperature ranges to further investigate the impact of temperature on RM partitioning. Linear regressions of $\log(1/K_p)$ as a function of $1/T$ in different seasons are shown in Fig. 2b. The correlation between K_p and T was close in winter ($R^2 = 0.93$, $P < 0.001$), followed by autumn and spring ($R^2 = 0.72$ and 0.67 , $P < 0.001$), and relatively weak in summer ($R^2 = 0.15$, $P = 0.11$). It is clear that the correlation was more remarkable in lower T and temperature explained more for K_p in the colder environments. The line's slope was the highest in winter, the lowest in summer, and similarly moderate in spring and autumn. Increased slope in winter suggests that RM transferred from gas to particle phase more quickly in the colder season.

3.2.2. Impact of aerosol compositions on RM partitioning

Aerosol chemical compositions might account for a part of K_p variance. In addition, the seasonal variation of slope of $\log(1/K_p)$ model was probably related to aerosol compositions (Rutter and Schauer, 2007b). Aerosol chemical compositions of NR-PM₁ were used to explore the impact of aerosol compositions on gas-particle partitioning of RM, since the synchronized data of PM_{2.5} compositions were unobtainable. In this study, a close correlation was observed between NR-PM₁ and PM_{2.5} concentrations ($R^2 = 0.52$, $P < 0.05$, Fig. S3a). The difference of chemical compositions between PM₁ and PM_{2.5} have been characterized

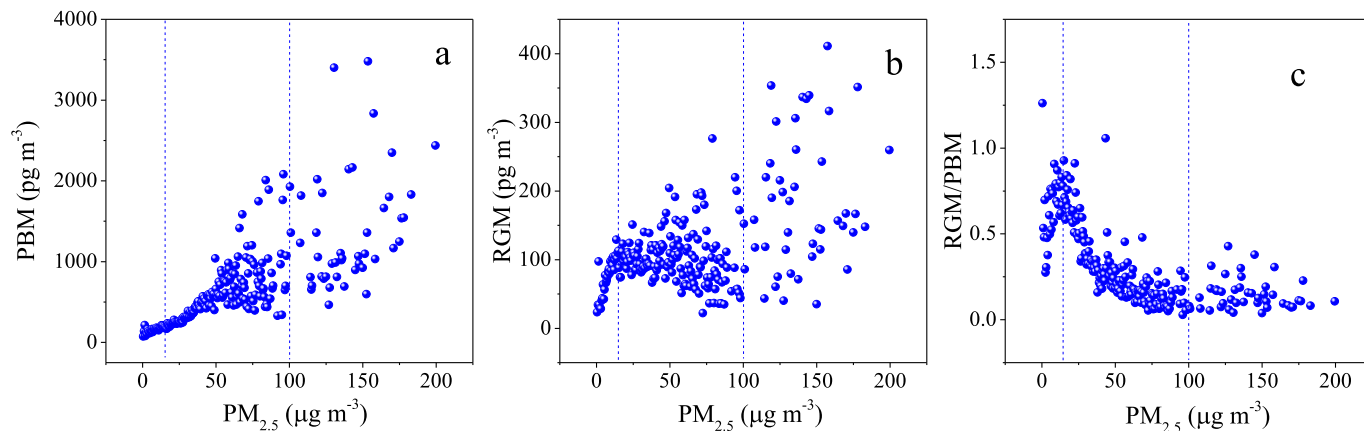


Fig. 1. Relationship of PBM (a), RGM (b), and RGM/PBM ratio (c) with $PM_{2.5}$. The dash lines represent the $PM_{2.5}$ concentrations of $15 \mu g m^{-3}$ and $100 \mu g m^{-3}$, respectively.

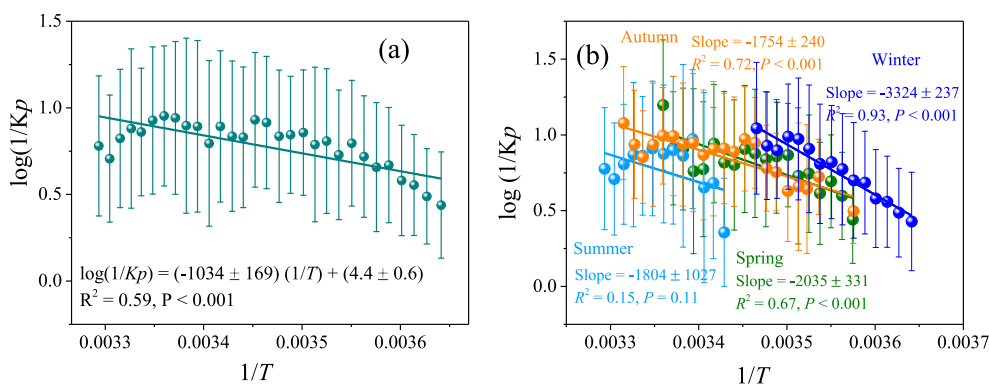


Fig. 2. Regression analyses of $\log(1/K_p)$ as a function of $1/T$ (a) during the whole study period and (b) in different seasons.

Table 3
Regression equations of $\log(1/K_p)$ as a function of $1/T$ in Ningbo and other areas.

Period	Interval of K_p	Regression equation	R^2	T range (°C)	Reference
Ningbo, China	2 h	$\log(1/K_p) = (-1034 \pm 169)(1/T) + (4.4 \pm 0.6)$	0.59	-0.8–34.6	This study
Beijing, China	2 h	$\log(1/K_p) = -1082(1/T) + 5$	0.24		Zhang et al. (2019)
Yongheung Island, Korea ^a	12 h	$\log(1/K_p) = -3362.7(1/T) + 13.5$	0.18		Lee et al. (2016)
5 North America sites	24 h	$\log(1/K_p) = -2500(1/T) + 10$	0.49		Amos et al. (2012)
2 North American sites	2–4 h	$\log(1/K_p) = -3485(1/T) + 13$	0.55	-17–33	Cheng et al. (2014)
Urban sites in USA	24 h	$\log(1/K_p) = -1710(1/T) + 7$	0.49		Rutter and Schauer (2007a)
Urban sites in USA ¹	24 h	$\log(1/K_p) = -4250(1/T) + 15$	0.77		

^a Filter-based method. Tekran method for others.

by previous studies. For example, a study based on filter measurement found that the contribution differences of chemical species (like organic matter, SO_4 , NO_3 , NH_4 , and Chl) between PM_1 and $PM_{2.5}$ were less than 4% (Zhao et al., 2017). The difference in chemistry between PM_1 and

$PM_{2.5}$ measured by aerosol mass spectrometers was not very consistent in previous studies (Zhang et al., 2017b; Sun et al., 2019). However, it is agreed that the chemical difference was affected by the level of PM concentration and RH. The latest study found that the contribution differences of chemical species became large under the highly polluted events and fog period (Sun et al., 2019, Fig. S3b). In this study, the $PM_{2.5}$ values rarely exceeded $100 \mu g m^{-3}$ (Fig. S3a) and the frequency of fog (RH = 100%) was less than 20%. Therefore, it could be speculated a comparable contribution of chemical species between PM_1 and $PM_{2.5}$.

To be more clear, the K_p values during the period of aerosol compositions observation were grouped into 17 intervals (<0.02 , $0.02-0.04$, $0.04-0.06$, $0.06-0.08$, $0.08-0.1$, $0.1-0.12$, $0.12-0.14$, $0.14-0.16$, $0.16-0.18$, $0.18-0.2$, $0.2-0.25$, $0.25-0.3$, $0.3-0.35$, $0.35-0.4$, $0.4-0.6$, $0.6-0.8$, $>0.8 m^3 \mu g^{-1}$) and each K_p interval contained 84–260 K_p values (2978 K_p in total). The relationships between K_p intervals and aerosol compositions are shown in Fig. 3 and Fig. S4. The K_p generally increased with the increasing fraction of Org in aerosols (Fig. S4) and they had a close relationship ($R^2 = 0.40$, $P < 0.05$). A field study in Shanghai, China also reported that PBM was strongly correlated with carbonaceous components (Duan et al., 2016). It has been indicated that carbonaceous components could enhance the transformation of air pollutants through heterogeneous reactions (Song et al., 2012; Han et al., 2018). Therefore, the positive correlation between Org and K_p in this study suggests that RM trended to partition toward particle phase with more organic fraction.

As showed in Fig. S4, the K_p generally increased with increasing fractions of NO_3 and Chl in aerosols. K_p was observed to be positively correlated with NO_3 and Chl ($R^2 = 0.27$ and 0.34 , $P < 0.05$). A positive correlation between K_p and Chl was also observed in Beijing based on

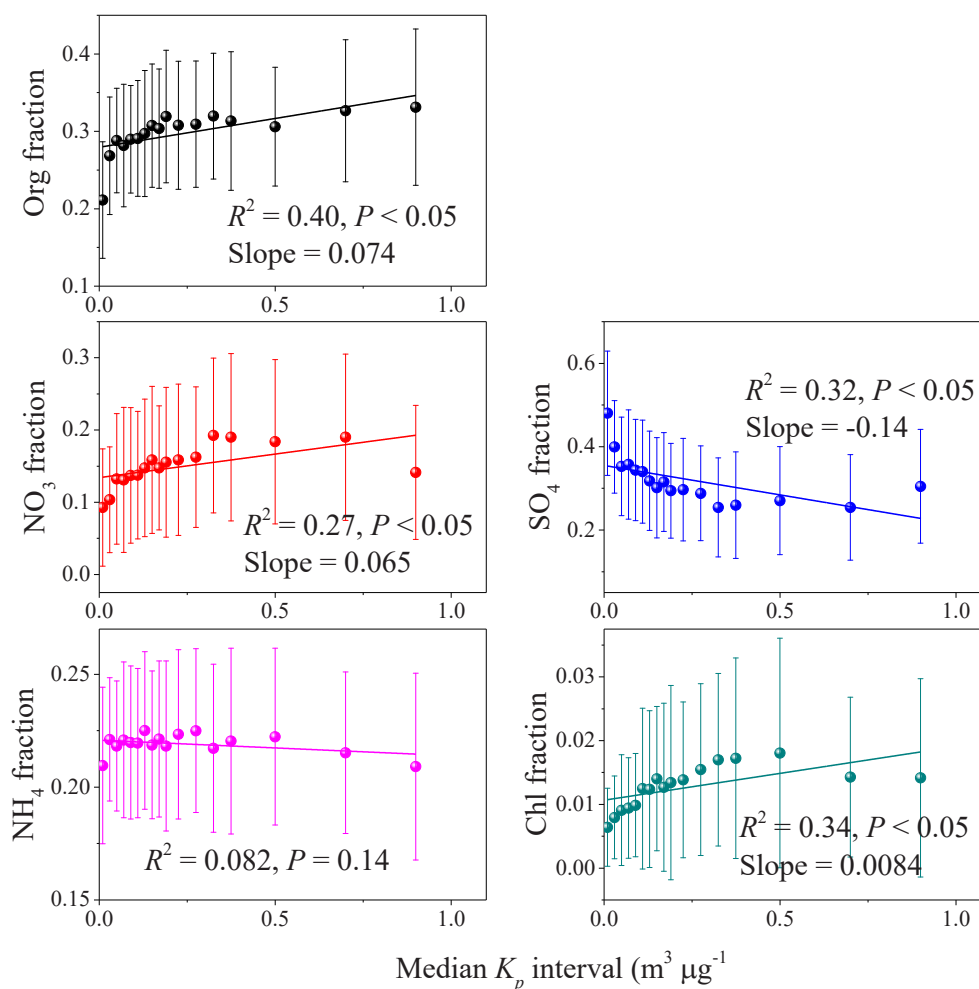


Fig. 3. Relationships between the fractions of aerosol chemical components and K_p .

filter measurements (Zhang et al., 2019). On the other hand, the K_p mostly increased with the decreasing fraction of SO_4 and their correlation was significantly negative ($R^2 = 0.32$, $P < 0.05$). The correlation between K_p and NH_4 was also negative. Our study confirms the results of Rutter and Schauer (2007b) in the laboratory which reported that nitrate and chloride particles had high K_p and ammonium sulfate had low K_p .

In this study, Org, NO_3 , and Chl were abundant in particles in spring and winter (Table S3), which were beneficial to RM partition toward particle phase. While in summer and autumn, particles were characterized by more SO_4 and NH_4 , which tended to partition RM toward gas phase. Accordingly, increases of chemical components beneficial for RM partitioning toward to particle phase could explain the higher slope of $\log(1/K_p)$ model in winter, and the reverse happened in summer.

3.3. Contribution of RM partitioning to PBM

As mentioned above, PBM was closely correlated with GEM and gas pollutants, such as SO_2 and NO_2 , indicating an important contribution of primary emissions to PBM. In addition, the adsorption of RGM onto particle is one of the well-known sources of PBM, which was different among the seasons relating to temperature and aerosol compositions. PCA-MLR was conducted to evaluate the contributions of potential sources to PBM. As a result, two principle factors with eigenvalues higher than 1 were extracted (Table S4). One factor (F1) explaining 49.1% of variance was characterized by air pollutants and PBM. As we know, SO_2 is a tracer for coal combustion, NO_2 is considered as an

indicator of traffic emissions, while CO mainly comes from burning of fossil fuels. Therefore, this factor was considered as direct emissions from sectional anthropogenic sources. The other factor (F2) explained 14.8% of variance and showed high loadings of K_p and moderate loadings of PBM and PM, which could be interpreted as the formation of PBM via gas-particle partitioning of RM. The two factors accounted for 64.0% of total variance and the rest might be attributed to natural sources and unidentified anthropogenic sources. Nonferrous smelters and cement production are considered to be two main sources of PBM in China (Zhang et al., 2015), but their typical tracers could not be involved in the PCA analysis of this study. Despite all this, the two factors identified as sectional primary emissions and RM partitioning were analyzed using MLR.

The formation of PBM via gas-particle partitioning of RM probably has an important contribution to PBM in the atmosphere as the YRD region of China is severely particle polluted. MLR analysis was applied on the PCA factor scores to evaluate the contribution of RM partitioning to PBM among different seasons. The correlation between observed and re-constructed PBM was close ($R^2 = 0.58$), suggesting the results of PCA-MLR were reliable. The MLR results for PBM during the four seasons are shown in Table 4. The correlation coefficient R^2 of regression equations was higher in autumn and winter than in spring and summer. Thus, the two sources explained variations of PBM more in the colder seasons. For the part of explainable PBM, sectional primary emissions had a remarkably higher contribution of 71.7% compared to RM partitioning (28.3%) in summer. Whereas, sectional primary emissions and RM partitioning relatively contributed 60.8% and 39.2% to PBM in winter,

Table 4

Multiple linear regression results for PBM in different seasons (F1: Sectional primary emissions, F2: RM partitioning).

Seasons	MLR Equation (adjusted R^2 , Sig.)	Contribution
Spring	$Z = 0.615 \cdot F1 + 0.239 \cdot F2$ (0.416, 0.000)	F1, 72.0% F2, 28.0%
Summer	$Z = 0.603 \cdot F1 + 0.238 \cdot F2$ (0.394, 0.000)	F1, 71.7% F2, 28.3%
Autumn	$Z = 0.691 \cdot F1 + 0.313 \cdot F2$ (0.681, 0.000)	F1, 68.8% F2, 31.2%
Winter	$Z = 0.735 \cdot F1 + 0.474 \cdot F2$ (0.615, 0.000)	F1, 60.8% F2, 39.2%

respectively. The relative contribution of RM partitioning to PBM showed an obviously increase from 28.0% in spring and 28.3% in summer to 31.2% in autumn and 39.2% in winter. As we know, intense human activities such as coal combustion in winter would increase the emission of PBM to the atmosphere. On the other hand, the formation of PBM via RM partitioning also enhanced in the cold season as mentioned above. Our results suggest that enhanced RM partitioning due to beneficial temperature and aerosol compositions in winter mostly weaken the relative contribution of primary emissions to PBM.

4. Conclusion

This study focused on the role of gas-particle partitioning of RM in the variations of PBM and RGM was conducted in Ningbo. Averaged concentrations of PBM and RGM were $316 \pm 377 \text{ pg m}^{-3}$ and $100 \pm 123 \text{ pg m}^{-3}$, respectively. The average fraction of PBM in RM was 73% and the ratio of RGM/PBM was the highest in summer (0.73 ± 1.31) and the lowest in winter (0.35 ± 0.56). Partitioning of RM between gas and particle phases was affected by $\text{PM}_{2.5}$ concentration. When $\text{PM}_{2.5}$ fell in the range of $15\text{--}100 \text{ } \mu\text{g m}^{-3}$, the conversion of RGM to PBM was enhanced as $\text{PM}_{2.5}$ increased. The partitioning of RM was strongly dependent on temperature and aerosol chemical compositions. An empirical relationship of K_p as a function of T developed over the combined data was $\log(1/K_p) = (-1034 \pm 169)(1/T) + (4.4 \pm 0.6)$. The relationship between K_p and T was obviously different among the seasons. T explained more for K_p and RM transferred quickly to particle phase in the cold season. On the other hand, RM trended to partition toward particle phase with more Org, NO_3 and Chl fractions, while RM trended to partition toward gas phase when particles were abundant in SO_4 and NH_4 . The relative contribution of gas-particle partitioning of RM to PBM varied among the seasons, with 28.0% to in spring, 28.3% in summer, 31.2% in autumn, and 39.2% in winter. Whereas, the relative contributions of sectional primary emissions to PBM were 71.7% in summer and 60.8% in winter. Benefiting from low temperature and abundant Org, NO_3 and Chl in aerosols, RM partitioning toward particle phase was enhanced and mostly weaken the relative contribution of primary emissions to PBM in cold seasons.

Declaration of competing interest

The authors declare that they have no known competing financial interests or personal relationships that could have appeared to influence the work reported in this paper.

CRediT authorship contribution statement

Lingling Xu: Conceptualization, Validation, Formal analysis, Writing - original draft, Writing - review & editing. **Yanru Zhang:** Data curation, Formal analysis. **Lei Tong:** Investigation, Project administration. **Yuping Chen:** Writing - review & editing. **Guoqing Zhao:** Investigation. **Youwei Hong:** Writing - review & editing, Validation. **Hang Xiao:** Writing - review & editing. **Jinsheng Chen:** Conceptualization, Resources, Supervision, Funding acquisition.

Acknowledgements

This research was financially supported by National Natural Science Foundation of China (No. 21507127; 41575146 & U1405235), Natural Science Foundation of Fujian province (2016J05050), the National Key Research and Development Program (2016YFC02005 & 2016YFC0112200), and Xiamen Atmospheric Environment Observation and Research Station of Fujian Province.

Appendix A. Supplementary data

Supplementary data to this article can be found online at <https://doi.org/10.1016/j.atmosenv.2020.117744>.

References

- Amos, H.M., Jacob, D.J., Holmes, C.D., Fisher, J.A., Wang, Q., Yantosca, R.M., Corbitt, E. S., Galarneau, E., Rutter, A.P., Gustin, M.S., Steffen, A., Schauer, J.J., Graydon, J.A., Louis, V.L.S., Talbot, R.W., Edgerton, E.S., Zhang, Y., Sunderland, E.M., 2012. Gas-particle partitioning of atmospheric Hg(II) and its effect on global mercury deposition. *Atmos. Chem. Phys.* 12, 591–603.
- Arctic Monitoring and Assessment Programme (Amap) and United Nations Environment Programme (Unep), 2013. Technical Background Report for the Global Mercury Assessment 2013. UNEP Chemicals Branch.
- Bash, J.O., Carlton, A.G., Hutzell, W.T., Bullock, O.R., 2014. Regional air quality model application of the aqueous-phase photo reduction of atmospheric oxidized mercury by dicarboxylic acids. *Atmosphere* 5, 1–15.
- Cheng, I., Zhang, L., Blanchard, P., 2014. Regression modeling of gas-particle partitioning of atmospheric oxidized mercury from temperature data. *J. Geophys. Res. Atmos.* 119, 11864–11876.
- Choi, H.-D., Huang, J.Y., Mondal, S., Holsen, T.M., 2013. Variation in concentrations of three mercury (Hg) forms at a rural and a suburban site in New York State. *Sci. Total Environ.* 448, 96–106.
- Duan, L., Xiu, G.L., Feng, L., Cheng, N., Wang, C.G., 2016. The mercury species and their association with carbonaceous compositions, bromine and iodine in $\text{PM}_{2.5}$ in Shanghai. *Chemosphere* 146, 263–271.
- Duan, L., Wang, X.H., Wang, D.F., Duan, Y.S., Cheng, N., Xiu, G.L., 2017. Atmospheric mercury speciation in Shanghai, China. *Sci. Total Environ.* 578, 460–468.
- Gustin, M.S., Amos, H.M., Huang, J., Miller, M.B., Heidecorn, K., 2015. Measuring and modeling mercury in the atmosphere: a critical review. *Atmos. Chem. Phys.* 15, 5697–5713.
- Han, Y.J., Kim, J.E., Kim, P.R., Kim, W.J., Yi, S.M., Seo, Y.S., Kim, S.H., 2014. General trends of atmospheric mercury concentrations in urban and rural areas in Korea and characteristics of high-concentration events. *Atmos. Environ.* 94, 754–764.
- Han, D.M., Zhang, J.Q., Hu, Z.H., Ma, Y.G., Duan, Y.S., Han, Y., Chen, X.J., Zhou, Y., Cheng, J.P., Wang, W.H., 2018. Particulate mercury in ambient air in Shanghai, China: size-specific distribution, gas-particle partitioning, and association with carbonaceous composition. *Environ. Pollut.* 238, 543–553.
- Huang, J.Y., Miller, M.B., Weiss-Penzias, P., Gustin, M.S., 2013. Comparison of gaseous oxidized Hg measured by KCl-coated denuders, and nylon and cation exchange membranes. *Environ. Sci. Technol.* 47, 7307–7316.
- Holmes, C.D., Jacob, D.J., Corbitt, E.S., Mao, J., Yang, X., Talbot, R., Slemr, F., 2010. Global atmospheric model for mercury including oxidation by bromine atoms. *Atmos. Chem. Phys.* 10, 12037–12057.
- Hong, Y.W., Chen, J.S., Deng, J.J., Tong, L., Xu, L.L., Niu, Z.C., Yin, L.Q., Chen, Y.T., Hong, Z.Y., 2016. Pattern of atmospheric mercury speciation during episodes of elevated $\text{PM}_{2.5}$ levels in a coastal city in the Yangtze River Delta, China. *Environ. Pollut.* 218, 259–268.
- Jaffe, D.A., Lyman, S., Amos, H.M., Gustin, M.S., Huang, J.Y., Selin, N.E., Levin, L., ter Schure, A., Mason, R.P., Talbot, R., Rutter, A., Finley, B., Jaegle, L., Shah, V., McClure, C., Arnbrose, J., Gratz, L., Lindberg, S., Weiss-Penzias, P., Sheu, G.R., Feddersen, D., Horvat, M., Dastoor, A., Hynes, A.J., Mao, H.T., Sonke, J.E., Slemr, F., Fisher, J.A., Ebinghaus, R., Zhang, Y.X., Edwards, G., 2014. Progress on understanding atmospheric mercury hampered by uncertain measurements. *Environ. Sci. Technol.* 48, 7204–7206.
- Landis, M.S., Stevens, R.K., Schaedlich, F., Prestbo, E.M., 2002. Development and characterization of an annular denuder methodology for the measurement of divalent inorganic reactive gaseous mercury in ambient air. *Environ. Sci. Technol.* 36, 3000–3009.
- Lee, G.S., Kim, P.R., Han, Y.J., Holsen, T.M., Seo, Y.S., Yi, S.M., 2016. Atmospheric speciated mercury concentrations on an island between China and Korea: sources and transport pathways. *Atmos. Chem. Phys.* 16, 4119–4133.
- Liu, B., Keeler, G.J., Timothy Dvonch, J., Barres, J.A., Lynam, M.M., Marsik, F.J., Morgan, J.T., 2010. Urban-rural differences in atmospheric mercury speciation. *Atmos. Environ.* 44, 2013–2023.
- Lynam, M.M., Keeler, G.J., 2005. Automated speciated mercury measurements in Michigan. *Environ. Sci. Technol.* 39, 9253–9562.
- Pankow, J.F., 1992. Application of common y-intercept regression parameters for log K_p vs $1/T$ for predicting gas-particle partitioning in the urban environment. *Atmos. Environ. Gen. Top* 26 (14), 2489–2497.

- Qin, X.F., Wang, X.H., Shi, Y.J., Yu, G.Y., Zhao, N., Lin, Y.F., Fu, Q.Y., Wang, D.F., Xie, Z. Q., Deng, C.R., Huang, K., 2019. Characteristics of atmospheric mercury in a suburban area of east China: sources, formation mechanisms, and regional transport. *Atmos. Chem. Phys.* 19, 5623–5940.
- Rutter, A.P., Schauer, J.J., 2007a. The effect of temperature on the gas-particle partitioning of reactive mercury in atmospheric aerosols. *Atmos. Environ.* 41, 8647–8657.
- Rutter, A.P., Schauer, J.J., 2007b. The impact of aerosol composition on the particle to gas partitioning of reactive mercury. *Environ. Sci. Technol.* 41, 3934–3939.
- Schroeder, W.H., Munthe, J., 1998. Atmospheric mercury—An overview. *Atmos. Environ.* 32, 809–822.
- Seinfeld, J.H., Pandis, S.N., 2006. *Atmospheric Chemistry and Physics: from Air Pollution to Climate Change*, second ed. John Wiley & Sons, Inc., Hoboken, New Jersey, USA.
- Song, H., Shang, J., Zhu, T., Zhao, L., Ye, J.H., 2012. Heterogeneous oxidation of SO₂ by Ozone on the surface of black carbon particles. *Chem. J. Chin. Univ.* 33, 2295–2302.
- Steffen, A., Lehnher, L., Cole, A., Ariya, P., Dastoor, A., Durnford, D., Kirk, J., Pilote, M., 2015. Atmospheric mercury measurements in the Canadian Arctic Part 1: a review of recent field measurements. *Sci. Total Environ.* 509–510, 3–15.
- Sun, Y.L., Wang, Z.F., Dong, H.B., Yang, T., Li, J., Pan, X.L., Chen, P., Jayne, J.T., 2012. Characterization of summer organic and inorganic aerosols in Beijing, China with an aerosol chemical speciation monitor. *Atmos. Environ.* 51, 250–259.
- Sun, Y.L., He, Y., Kuang, Y., Xu, W.Y., Song, S.J., Ma, N., Tao, J.C., Cheng, P., Wu, C., Su, H., Cheng, Y.F., Xie, C.H., Chen, C., Lei, L., Qiu, Y.M., Fu, P.Q., Croteau, P., Worsnop, D.R., 2019. Chemical differences between PM₁ and PM_{2.5} in highly polluted environment and implications in air pollution studies. *Geophys. Res. Lett.* 47, e2019GL086288.
- Talbot, R., Mao, H.T., Feddersen, D., Smith, M., Kim, S.Y., Sive, B., Haase, K., Ambrose, J., Zhou, Y., Russo, R., 2011. Comparison of particulate mercury measured with manual and automated methods. *Atmosphere* 2 (1), 1–20.
- Xu, L.L., Chen, J.S., Yang, L.M., Niu, Z.C., Tong, L., Yin, L.Q., Chen, Y.T., 2015. Characteristics and sources of atmospheric mercury speciation in a coastal city, Xiamen, China. *Chemosphere* 119, 530–539.
- Yi, H., Tong, L., Lin, J.M., Cai, Q.L., Wang, K.Q., Dai, S.R., Li, J.R., Chen, J.S., Xiao, H., 2020. Temporal variation and long-range transport of gaseous elemental mercury (GEM) over a coastal site of East China. *Atmos. Res.* 233, 104699.
- Zhang, L., Wang, S.X., Wang, L., Hao, J.M., 2013. Atmospheric mercury concentration and chemical speciation at a rural site in Beijing, China: implications of mercury emission sources. *Atmos. Chem. Phys.* 13, 10505–10516.
- Zhang, L., Wang, S.X., Wang, L., Wu, Y., Duan, L., Wu, Q.R., Wang, F.Y., Yang, M., Yang, H., Hao, J.M., Liu, X., 2015. Updated emission inventories for speciated atmospheric mercury from anthropogenic sources in China. *Environ. Sci. Technol.* 49, 3185–3194.
- Zhang, L., Wang, L., Wang, S.X., Dou, H.Y., Li, J.F., Li, S., Hao, J.M., 2017a. Characteristics and sources of speciated atmospheric mercury at a coastal site in the East China Sea Region. *Aerosol Air Qual. Res.* 17, 2913–2923.
- Zhang, Y.J., Tang, L.L., Croteau, P.L., Favez, O., Sun, Y.L., Canagaratna, M.R., Wang, Z., Couvidat, F., Albinet, A., Zhang, H.L., Sciare, J., Prévôt, A.S.H., Jayne, J.T., Worsnop, D.R., 2017b. Field characterization of the PM_{2.5} aerosol chemical speciation monitor: insights into the composition, sources, and processes of fine particles in eastern China. *Atmos. Chem. Phys.* 17, 14501–14517.
- Zhang, H., Wang, Z.W., Wang, C.J., Zhang, X.S., 2019. Concentrations and gas-particle partitioning of atmospheric reactive mercury at an urban site in Beijing, China. *Environ. Pollut.* 249, 13–23.
- Zhao, T., Yang, L.X., Yan, W.D., Zhang, J.M., Lu, W., Yang, Y.M., Chen, J.M., Wang, W.X., 2017. Chemical characteristics of PM₁/PM_{2.5} and influence on visual range at the summit of Mount Tai, North China. *Sci. Total Environ.* 575, 458–466.